

## Strain-induced growth-mode transition of V in epitaxial Mo/V(001) superlattices

J. Birch,\* L. Hultman, and J.-E. Sundgren

*Thin Film Physics Division, Department of Physics, Linköping University, S-581 83 Linköping, Sweden*

G. Radnoczi

*Research Institute of Technical Physics, H-1325 Budapest, P.O. Box 76, Hungary*

(Received 28 November 1994; revised manuscript received 31 October 1995)

Epitaxial (001) oriented Mo/V superlattices have been grown on MgO (001) substrates kept at 700 °C by magnetron sputter deposition. Films with different modulation periods  $\Lambda$  and with different fractions,  $X_V$ , of V in the period were investigated ( $X_V = D_V/\Lambda$ , where  $D_V$  is the V-layer thickness). The  $\Lambda$  range was 0.313 to 17.7 nm and  $X_V$  was varied in the range 0.11 to 0.93. The as-deposited films were characterized by cross-sectional transmission-electron microscopy and by x-ray-diffraction techniques. The results show that the superlattices change from a structure with smooth Mo and V layers with sharp and well-defined layer interfaces to a structure where the V layers have a large in-plane thickness fluctuation when the V layers exceed a critical thickness  $D_c$ .  $D_c$  increases from  $\sim 0.3$  to  $\sim 8$  nm as  $X_V$  is increased from 0.11 to 0.83 and for equally thick Mo and V layers  $D_c$  is  $\sim 2.5$  nm. The layer thickness fluctuations are nonaccumulative and disappear if the periodicity of a growing Mo/V superlattice is changed so that the V-layer thickness becomes smaller than  $D_c$ . Mo was found to grow in a two-dimensional mode producing layers with uniform thicknesses, following the undulated surface of the V layers. The results are explained in terms of growth above and below the roughening temperatures for V and Mo, respectively. The roughening of V is suggested to be triggered by the surface strain and curvature induced by misfit dislocations.

### I. INTRODUCTION

The use of one-dimensional superlattice structures is rapidly expanding due to their application in, e.g., semiconductor devices and in magnetic recording media. The latter application area has in fact been the main driving force for the increasing interest in structure and properties of ultrathin metallic films and multilayers. The need for an increased fundamental understanding, and thus control, of film nucleation and growth processes is thus understandable. The details of how growth proceeds in a particular case depends on both the thermodynamics and the kinetics involved. For example, at high temperatures where surface diffusion is extensive, the wetting of a surface by deposited atoms largely depends on the energies of the substrate-vacuum, film-vacuum, and substrate-film interfaces,  $\gamma_s$ ,  $\gamma_f$ , and  $\gamma_i$ , respectively. Neglecting anisotropy of the surface energies and any kinetic barriers, the deposit wets the substrate and nucleates in a two-dimensional (2D) mode if  $\gamma_i + \gamma_f < \gamma_s$ . On the other hand if  $\gamma_i + \gamma_f \approx \gamma_s$  the film growth is expected to change to a three-dimensional (3D) mode after a few monolayers,<sup>1-3</sup> i.e., the film grows in a so-called Stranski-Krastanow (SK) mode, commonly observed in many heteroepitaxial materials system. Finally, if  $\gamma_i + \gamma_f > \gamma_s$  a 3D island growth mode is expected to occur directly.

However, as mentioned above, kinetic effects such as high supersaturation, kinetic energy barriers at surface steps, etc. can significantly influence the growth mode. Also the presence of strains in heterostructures with a lattice mismatch between the two constituents will influence the growth in terms of the interface structure and microstructure of the deposited layers. This is of particular importance in superlattice structures since the total strain not only depends on the con-

stituent materials but also on the ratio of the layer thicknesses and the amount of structural defects. The strain energy in a growing film that has a lattice mismatch to the substrate increases linearly with film thickness. This continues until a critical thickness has been reached large enough such that the built-in strain energy can act as a driving force for relaxation of the coherency strain. This can be done either close to the interface by introduction of misfit dislocations<sup>4</sup> (MD) or by rearrangement of the film atoms to form 3D islands. Such islands can either be coherent at the interface but relaxed at the surface<sup>5,6</sup> or fully relaxed by MD's at their interface to the substrate.<sup>3,7-9</sup> Relaxed 3D island growth, also called SK growth, can occur when the film-substrate interaction is weak, compared to the interaction between atoms in the film only,<sup>3</sup> and when there is a lattice mismatch between the film and the substrate.<sup>1</sup> The thickness where the growth turns from 2D to 3D in SK growth is not easy to predict but it is usually found to be a few monolayers only. Coherent 3D island (CI) growth has been observed in several heteroepitaxial semiconductor systems.<sup>5,6,10-12</sup> This growth mode is possible when the diffusion of surface atoms is not limited by kinetics and if there exists a barrier for the creation of MD's. The underlying mechanism for this growth mode is a spontaneous long-range 3D surface evolution that occurs at the surface of a strained solid.<sup>13-15</sup> For a growing film the 3D evolution of the surface can be suppressed up to a critical thickness  $D_{CI}$ .<sup>14</sup>

Whereas different theoretical models for all these strain relaxation mechanisms have been proposed,<sup>1,7,9,14,16,17</sup> there are still some features where realistic quantitative models as well as experimental data are rather limited. An example of the latter is the so-called roughening transition that occurs for flat metal surfaces as the temperature exceeds the rough-

ening temperature  $T_R$ .<sup>18–21</sup> Although the implications of the roughening transition on crystal growth were pointed out almost 45 years ago,<sup>18</sup> there has been surprisingly little investigation of it for crystal growth from the vapor phase and we believe that this effect has been neglected in many studies of epitaxial growth.

In this paper we report on growth, by magnetron sputtering, of (001) oriented epitaxial Mo/V superlattices on MgO(001) single-crystal substrates. The system was chosen as a model system of epitaxial metallic superlattices with a moderate lattice mismatch  $\eta_0$  between the two constituents. The lattice mismatch for V on Mo amounts to  $\eta_0 = -3.9\%$  and is defined as  $\eta_0 = (a_{0V} - a_{0Mo})/a_{0Mo}$ , where  $a_{0V}$  and  $a_{0Mo}$  are the bulk lattice parameters. In particular, we report on how the growth modes depend on the wavelength  $\Lambda$  and the fraction,  $X_V$ , of V in the period ( $X_V = D_V/\Lambda$  where  $D_V$  is the V-layer thickness) of grown structures. It is demonstrated that the ability to grow smooth layers with sharp interfaces (thus to avoid 3D growth) strongly depends on both  $\Lambda$  and  $X_V$ . The observed results are discussed in terms of existing models for strain relaxation and surface roughening. Furthermore, it is demonstrated that, for this material system, a roughness formed during growth of one layer does not necessarily accumulate, but that instead a smoothing can be obtained upon growth of subsequent layers.

## II. EXPERIMENTAL DETAILS

The Mo/V superlattices were grown epitaxially on polished MgO(001) wafers by dual target magnetron sputtering. The deposition system and the procedures for substrate cleaning and growth as described elsewhere<sup>22</sup> were used with the following exceptions: The substrates were mildly cleaned using soap and water before the ultrasonic cleaning procedure and they were introduced through a load-lock system into the deposition chamber. An ultimate pressure of  $\leq 3 \times 10^{-7}$  Pa ( $2 \times 10^{-9}$  Torr) was achieved after baking the Viton sealed chamber (24 h at 120 °C), which was equipped with a turbo molecular pump and an liquid-nitrogen-(LN<sub>2</sub>-) cooled titanium sublimation pump. Furthermore, the background pressure was always  $< 7 \times 10^{-6}$  Pa ( $5 \times 10^{-8}$  Torr) before initiating the growth, the Ar sputtering pressure was 0.4 Pa ( $3 \times 10^{-3}$  Torr), and the nominal deposition rates were kept at 0.10 nm/s as determined by quartz crystal monitors. The calibration of the quartz crystal monitors was frequently controlled using the method of asymmetric periods.<sup>23</sup> The substrate temperature  $T_S$  was kept at 973 K during the depositions and some of the samples were grown so that they contained two or more consecutively deposited superlattices with different  $\Lambda$  and  $X_V$ . The investigated  $\Lambda$  range was 0.313–17.7 nm and  $X_V$  was varied in the range 0.11–0.93.

Conventional  $\theta-2\theta$  powder x-ray diffraction (XRD) was carried out on the samples in the low-angle (reflectivity) region as well as in the high-angle region around the average Mo/V 002 peak (so-called Bragg peak). These measurements were performed using a Philips PW1820 powder diffractometer with an accuracy of  $0.01^\circ$  in  $2\theta$ . Reciprocal-space mapping (RSM) around the Mo/V 002 and 222 Bragg peaks was performed using a Philips MRD system operated with (low resolution) parallel-beam x-ray optics. By performing a sequence of coupled  $\omega-2\theta$  scans where the incidence angle

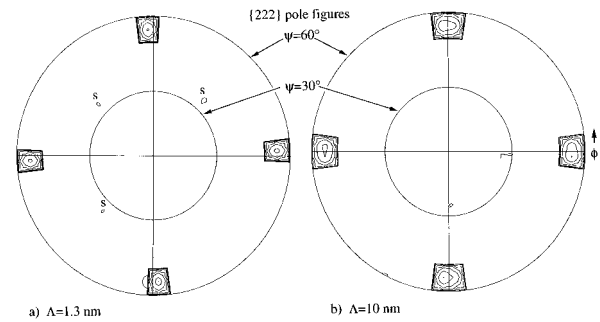


FIG. 1. Pole-figure plot of the average Mo/V {222} planes from two Mo/V superlattices with (a)  $\Lambda = 1.3$  nm and (b)  $\Lambda = 10.0$  nm. Three {112} substrate peaks are marked with an *s* in (a).

$\omega$  is offset by a small amount between each scan, a two-dimensional map of the intensity distribution in reciprocal space can be recorded. In this way the location of peaks can be determined accurately. The incident beam, which was produced by a Cu laboratory source, was collimated to  $0.35^\circ$  and the secondary optics consisted of a  $0.27^\circ$  parallel-plate collimator followed by a flat graphite secondary monochromator. The sample was mounted on an open Eulerian cradle with  $360^\circ$  freedom in the azimuthal angle  $\phi$  and  $100^\circ$  freedom in the tilt angle  $\psi$ , which tilts the sample normal with respect to the diffraction plane. A more detailed description of the RSM using this system is given elsewhere.<sup>24</sup> RSM made it possible to clearly distinguish the peaks corresponding to different superlattices in the same sample and the broadening of the Bragg peaks in different directions in reciprocal space could thus be measured for each superlattice. Texture pole figures were recorded for the average Mo/V {002}, {220}, and {222} lattice planes where the  $\phi$  and  $\psi$  ranges were  $0-360^\circ$  and  $0-85^\circ$ , respectively. Both angles were scanned in steps of  $5^\circ$ .

High-resolution (HR) cross-sectional transmission electron microscopy (XTEM) was carried out in a Jeol 4000EX microscope operated at 400 kV with a point-to-point resolution of 0.16 nm and conventional XTEM was done using a Philips CM20UT microscope operated at 200 kV. XTEM sample preparation was carried out using standard procedures.<sup>23</sup>

## III. RESULTS

The crystalline quality of the Mo/V(001) superlattices was investigated by performing a series of texture scans for three different average plane distances of the superlattices. Figure 1 shows the pole-figure plots up to  $\psi = 60^\circ$  of the Mo/V {222} planes from two superlattices, (a)  $\Lambda = 1.3$  nm (b)  $\Lambda = 10.0$  nm, both with  $X_V = 0.5$ . As can be seen, only four sharp peaks at the same  $\psi$  angle of  $\sim 54.7^\circ$  appear, separated from each other by  $90^\circ$  in  $\phi$ . No other peaks that could be related to the superlattices were found outside the range shown. Thus the films are epitaxial without the presence of high-angle grain boundaries.

The  $\theta-2\theta$  powder XRD patterns around the Mo/V 002 Bragg peaks from two symmetric ( $X_V \approx 0.5$ ) superlattices with  $\Lambda = 5.0$  and 7.2 nm are shown in Fig. 2. It can be seen that the superlattice with  $\Lambda = 5.0$  nm has a larger angular separation of the satellites and their relative intensities are

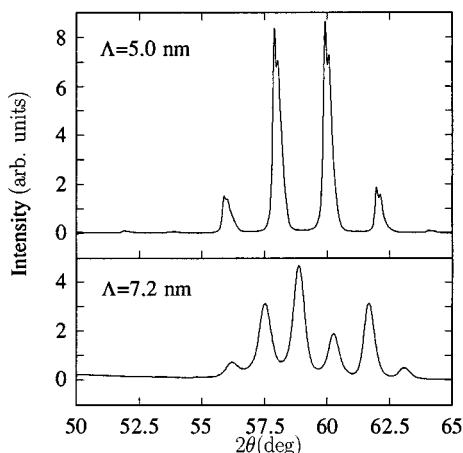


FIG. 2.  $\theta$ - $2\theta$  powder XRD patterns around the Mo/V 002 Bragg peaks from two symmetric ( $X_V \approx 0.5$ ) superlattices with  $\Lambda = 5.0$  and  $7.2$  nm.

very different in comparison to the sample with  $\Lambda = 7.2$  nm. These differences are mainly effects of the different periodicities of the samples. Furthermore, it can be seen that widths of the peaks are smaller for the short-period sample. The full width at half maximum,  $\beta_{2\theta}$ , of the 002 Bragg peaks from several symmetric samples with various periods are shown in Fig. 3. The  $\beta_{2\theta}$  values are corrected from the instrumental broadening ( $0.12^\circ 2\theta$ ) by quadratic subtraction and the solid line is drawn as a guide to the eye. An abrupt increase in  $\beta_{2\theta}$  can be seen when  $\Lambda$  is 5 nm. When  $\Lambda$  is smaller than 5 nm the largest value of  $\beta_{2\theta}$  is  $0.18^\circ 2\theta$  (marked by dotted lines in the figure) and when  $\Lambda$  exceeds 5.0 nm,  $\beta_{2\theta}$  increases to  $\sim 0.4^\circ 2\theta$ .

In order to relate the broadening of the XRD Bragg peaks to the microstructures of the samples XTEM was performed on samples with symmetric ( $X_V = 0.5$ ) periods in the range of 0.6–10 nm. Figure 4 shows XTEM images of a superlattice with  $\Lambda = 4.94$  nm and Fig. 5 shows XTEM images of a superlattice with  $\Lambda = 7.4$  nm. In each of Figs. 4 and 5, the upper and lower panels show overview and detailed lattice-resolved images, respectively. The superlattice with  $\Lambda = 4.94$  nm shows flat and smooth layers with sharp interfaces. Furthermore, the HR XTEM image of this superlattice clearly resolves the (002) and (110) lattice fringes in the

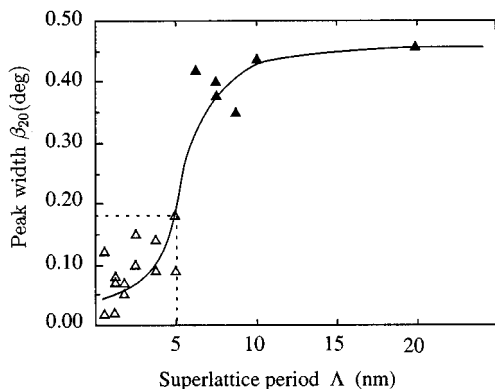


FIG. 3. The full width at half maximum,  $\beta_{2\theta}$ , of the Mo/V 002 Bragg peaks in symmetric ( $X_V \approx 0.5$ ) Mo/V superlattices as a function of  $\Lambda$ .

growth and in-plane directions, respectively, and also a few misfit dislocations (MD) can be observed. The dislocations are of edge type with the dislocation line  $\mathbf{u} = [1\bar{1}0]$  and Burgers vector  $\mathbf{b} = 1/2 \times [110]$  in the plane of the interfaces. The average distance between adjacent dislocations was 11.0 nm as determined by measurements in HR XTEM micrographs from different regions of the sample, altogether representing 760 nm of interface length with a TEM sample foil thickness of 20–50 nm. This dislocation density is equivalent to a strain relaxation  $\rho$  of  $\sim 50\%$ .  $\rho$  is defined for both Mo and V by  $a_{\parallel}(\rho) = a_0 + (a_{\parallel}^* - a_0)(1 - \rho)$  where  $a_{\parallel}$  is the actual lattice parameter parallel to the layers and  $a_{\parallel}^*$  is the lattice parameter common to both the Mo and V layers expected if no relaxation at all has occurred. The dislocations are predominantly located close to the interfaces, in the V layers. In contrast to this highly ordered structure, the superlattice with  $\Lambda = 7.4$  nm exhibits a large waviness of the layers and the crystal lattice is highly distorted. The wavy nature of the layers can be seen to have the origin in large thickness variations in each V layer (bright contrast) while the Mo layers (dark contrast) follow the wavy surface, keeping a constant layer thickness. In order to investigate this phenomenon in more detail, XTEM was performed on a specially designed multilayered superlattice with several consecutively deposited superlattices of different periods. The relative layer thicknesses were kept constant,  $X_V = 0.5$ , throughout the sample. The left part of Fig. 6 shows a schematic of this sample, which contains eight different superlattices with  $\Lambda$  ranging from 10.0 nm closest to the substrate down to 1.24 nm at the top of the sample. Also shown in Fig. 6 are two cross-sectional TEM micrographs from the short-period region (upper image) and the long-period region of the sample (lower image). In the upper image in Fig. 6 the boundary region between the superlattices with  $\Lambda = 2.40$  and 1.86 nm is shown and the lower image in Fig. 6 shows the boundary region between the superlattices with  $\Lambda = 10.0$  and 7.4 nm. Even though the waviness is less pronounced in this sample, compared to the sample shown in Fig. 5, it can be seen that the surface roughness of one V layer is not reproduced in the next V layer, i.e., the surface roughness is not correlated. On the contrary, the in-plane thickness fluctuations of the V layers, which occur for large  $\Lambda$ , are often seen to be correlated. Those parts of the V layers that are relatively thin are often directly followed by locally thick V layers. Furthermore, the conformal Mo coverage of the wavy V surface can also be seen in this sample. The short-period superlattices in Fig. 6, which were deposited on top of the wavy structures, exhibit very smooth layers. The TEM analysis showed that the transition from wavy to flat V layers occurred when  $\Lambda$  was changed from 7.4 to 5.0 nm in this sample. This coincides with the period where an abrupt increase in XRD peak width was observed. Thus, we conclude that the change in microstructure, observed by TEM, when  $\Lambda$  is increased is correlated to the increased XRD peak width observed when  $\Lambda$  exceeds 5 nm. The fact that the short-period superlattices grew with very flat layers on top of the wavy superlattices shows that the roughness of the V surface at a particular stage of the growth is not accumulated or increased as the growth proceeds and a smoothening mechanism between consecutive bilayers is involved. Hence, the layer-thickness fluctuations, referred to as waviness in the present work, is of

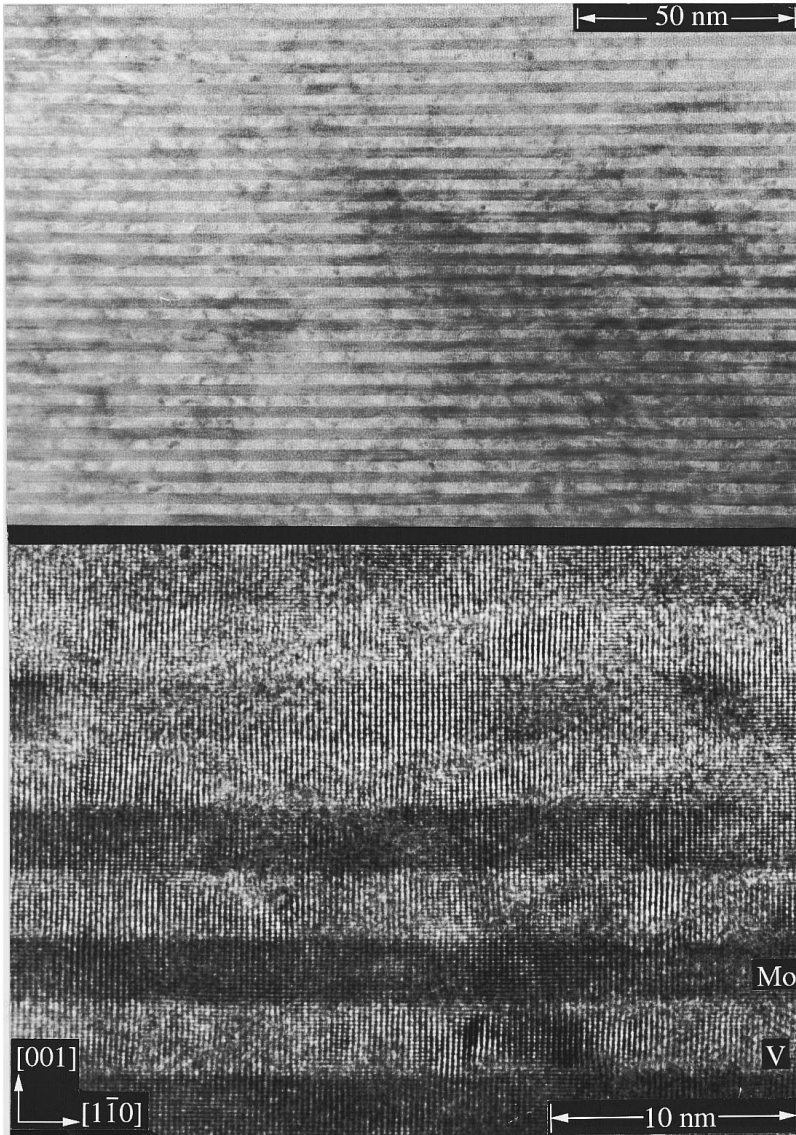


FIG. 4. Cross-sectional TEM images of a superlattice with  $\Lambda = 4.94$  nm and  $X_V = 0.5$ . The upper and lower panels show overview and detailed lattice resolved images, respectively.

a different origin than the cumulative layer-thickness fluctuations caused by low surface mobility and self-shadowing reported in several other studies.<sup>25–27</sup>

Multilayered superlattice films were also used in the XRD analyses in order to accurately determine the individual layer thicknesses in the different superlattices. This was done by the method of asymmetric superlattices<sup>23</sup> for a set of samples where each individual sample contained at least two different superlattices with different  $\Lambda$  and  $X_V$ . The two sets of overlapping superlattice peaks could be separated by RSM of the regions around the Mo/V 222 peaks. When each peak had been identified, the periods were determined and, knowing the duration of deposition of each layer, the deposition rates and the individual layer thicknesses were calculated by the method of asymmetric periods. As an example of this method, Fig. 7 shows two RSM's from the regions around (a) the Mo/V 002 and (b) the Mo/V 222 Bragg peaks from a sample containing two different superlattices with  $\Lambda_1 = 4.10$  nm,  $X_{V1} = 0.76$  and  $\Lambda_2 = 9.6$  nm,  $X_{V2} = 0.16$ , respectively. The intensity is mapped in reciprocal space with the axes in units of  $1/d$  ( $\text{\AA}^{-1}$ ) and with the  $x$  axis in the direction parallel to the sample surface and the  $y$  axis or-

thogonal to the surface (in the growth direction). The RSM around the 002 peaks shows many overlapping peaks. Several of the peaks are revealed only by a different width in the in-plane direction at low intensities. However, in the map around the 222 peaks, two sets of superlattice peaks are clearly isolated from each other. The Bragg peaks, marked  $B_1$  and  $B_2$ , corresponding to each of the superlattices, are in this case recognized by their large intensities. The superlattice satellites from each superlattice are seen as peaks equidistantly spaced in the growth direction in reciprocal space. These peaks are labeled  $\dots S_1^{-2}, S_1^{-1}, S_1^{+1}, S_1^{+2}, \dots$  and  $\dots S_2^{-2}, S_2^{-1}, S_2^{+1}, S_2^{+2}, \dots$  in the figure. When the peaks have been identified in the 222 map, then the small and overlapping features in the symmetric 002 map can be labeled. The peaks in  $\theta$ - $2\theta$  powder diffractograms, which have higher resolution than parallel-beam RSM, were identified in the same way and were used in order to get more accurate values of  $\Lambda_1$  and  $\Lambda_2$ .

The curve in Fig. 3 that shows how  $\beta_{2\theta}$  depends on  $\Lambda$  was obtained for symmetric superlattices ( $X_V \approx 0.5$ ). Furthermore, the  $\theta$ - $2\theta$  XRD patterns used for this result were

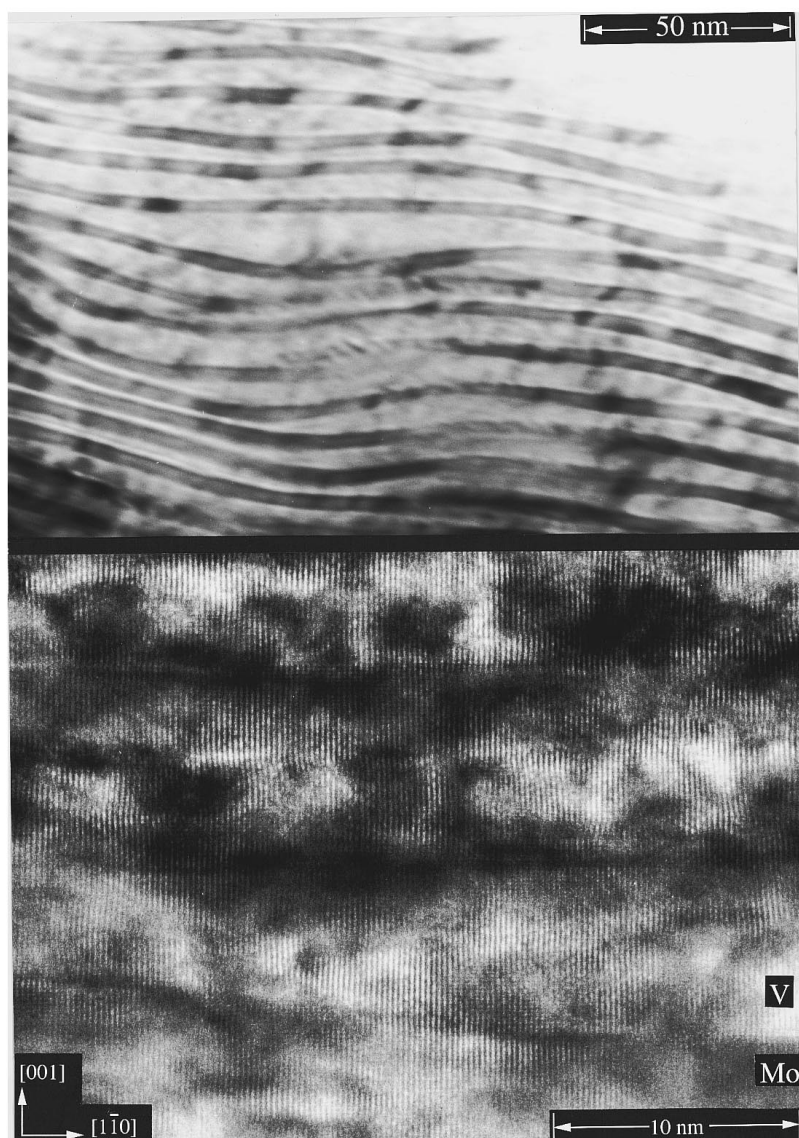


FIG. 5. Cross-sectional TEM images of a superlattice with  $\Lambda = 7.4$  nm and  $X_V = 0.5$ . The upper and lower panels show overview and detailed lattice resolved images, respectively.

obtained using a powder diffractometer with focusing Bragg-Brentano geometry, making it impossible to relate a small peak broadening to the crystallographic directions of a single-crystal sample. Using RSM it is possible to directly identify the direction of the peak broadening, making it easier to identify the features causing the broadening. The increased  $\theta$ - $2\theta$  broadening of the Bragg peaks observed in the Bragg-Brentano geometry (Figs. 2 and 3) was found to be related to an increased  $\omega$  broadening,  $\beta_\omega$  of the Bragg peaks in RSM. In order to investigate how the growth of V depends on  $\Lambda$  as well as on  $X_V$ , several multilayered superlattice samples, each containing at least two superlattices with different  $\Lambda$  and  $X_V$ , were investigated by RSM. The superlattices were classified into two groups depending on if the measured  $\beta_\omega$  was narrow ( $\beta_\omega < 0.41^\circ$ ) or if the Bragg peaks were wide ( $0.41^\circ < \beta_\omega$ ). The limit  $\beta_\omega = 0.41^\circ$  corresponds to the limit  $\beta_{2\theta} = 0.18^\circ$   $2\theta$  at  $\Lambda = 5.0$  nm marked by the dotted lines in Fig. 3. Figure 8 is a plot showing the result of this classification where  $X_V$  is plotted versus  $\Lambda$  and the symbols in the figure show which group each superlattice belongs to. The results in Fig. 3 lie on the line  $X_V \approx 0.5$ . A trend can be seen that superlattices that yield narrow Bragg

peaks have either large  $X_V$  or short  $\Lambda$  whereas superlattices with wide peaks have relatively small  $X_V$  values or large  $\Lambda$ . This result shows that V grows in a 2D fashion to larger layer thicknesses when the V fraction of the modulation period becomes larger. This, in turn, implies that for each particular asymmetry  $X_V$  of a Mo/V(001) superlattice, there is a critical V-layer thickness  $D_c$  (and periodicity  $\Lambda$ ) above which the x-ray peaks are broad, i.e., the growth of V is 3D in character. This can be seen in Fig. 9 where the dotted line shows  $D_c$  plotted versus  $X_V$  (labeled on the top of the figure). It can be seen that the transition between narrow and wide peaks increases monotonically with  $X_V$ , indicating that the 2D-3D transition occurs at a larger V-layer thickness if  $X_V$  is increased. When  $X_V = 0.5$  the transition occurs at  $D_V \approx 2$  nm, which is close to the value of 2.5 nm, obtained using the Bragg-Brentano XRD geometry and TEM. The other lines in Fig. 9 represent theoretical models for the critical thickness, which will be discussed in the next section.

In summary, the main results are as follows: (i) A transition from smooth to wavy V layers occurs at a critical V-layer thickness  $D_c$ . (ii)  $D_c$  increases when  $X_V$  increases. (iii) Growth with flat layers can be achieved on top of a

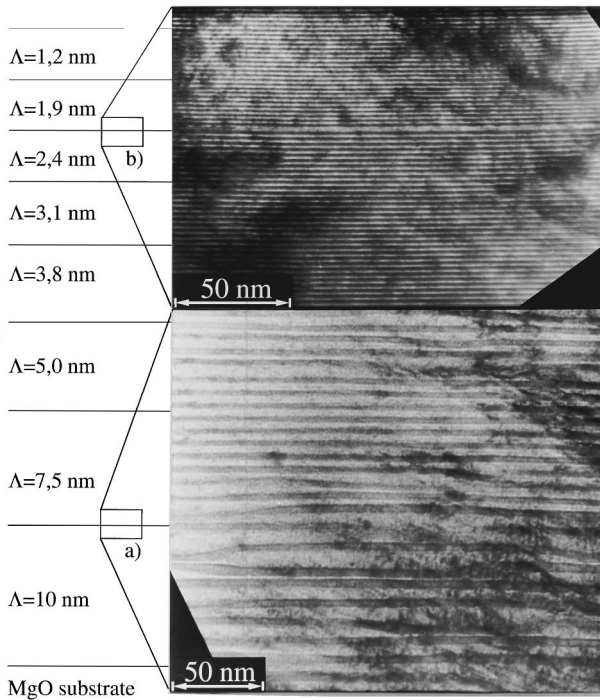


FIG. 6. A schematic figure of a multilayered superlattice sample, which contains eight different symmetric superlattices with  $\Lambda$  ranging from 10.0 nm closest to the substrate down to 1.24 nm at the top of the sample. The upper TEM micrograph shows the boundary region between the superlattices with  $\Lambda = 2.40$  and 1.86 nm and the lower image shows the boundary region between the superlattices with  $\Lambda = 10.0$  and 7.4 nm.

superlattice with wavy layers if the modulation is changed such that  $D_V < D_c$ . (iv) Mo does not show any tendency of 3D growth.

#### IV. DISCUSSION

We have experimentally observed, in single-crystal Mo/V(001) superlattices, that a transition from smooth to wavy V layers occurs at a critical V-layer thickness  $D_c$ , which for superlattices with symmetric periods is  $\sim 2.5$  nm. In contrary to this, Mo was found to grow with a uniform thickness following the surface of the V layers. The flat-wavy transition is associated with an increased XRD peak width of the superlattice Bragg peaks. The XRD analyses showed that  $D_c$  increases with increasing relative V-layer thickness  $X_V = D_V/\Lambda$ . The layer thickness fluctuations are nonaccumulative and disappear if the periodicity of a growing Mo/V superlattice is changed so that  $D_V$  becomes smaller than  $D_c$ . The results point at four phenomena occurring during growth of the superlattices; the transition from smooth V layers to layers with large in-plane thickness fluctuations as  $D_V$  exceeds  $D_c$ , the  $X_V$  dependence of  $D_c$ , the smoothing process responsible for the nonaccumulative surface roughness, and the conformal coverage of Mo on the wavy V surface.

In this section we first discuss the expected nucleation behavior of Mo and V in terms of surface and interface energies. Thereafter, possible reasons for a 3D morphology evolution of a growing V film are discussed. We conclude

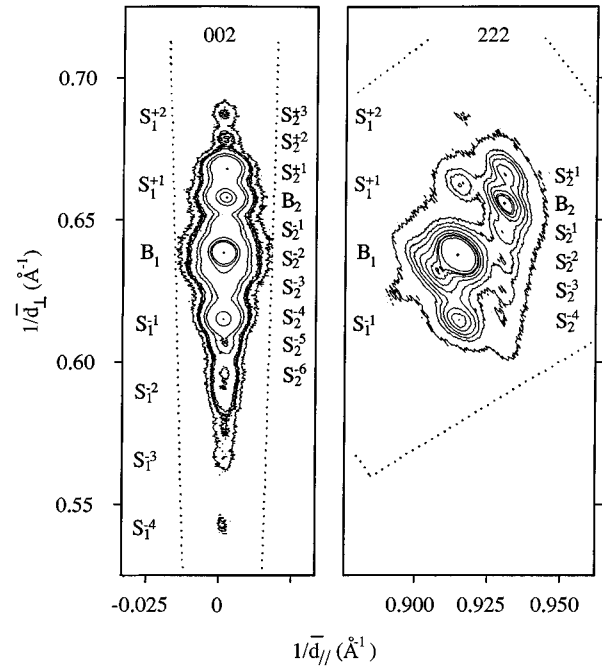


FIG. 7. Reciprocal-space maps from the regions around (a) the Mo/V 002 and (b) the Mo/V 222 Bragg peaks from a sample containing two different superlattices with  $\Lambda_1 = 4.10$  nm,  $X_{V1} = 0.76$  ( $D_{1Mo} = 0.99$  nm,  $D_{1V} = 3.11$  nm), and  $\Lambda_2 = 9.6$  nm,  $X_{V2} = 0.16$  ( $D_{2Mo} = 8.06$  nm,  $D_{2V} = 1.55$  nm), respectively. The intensity of the diffracted x-ray beam is mapped in reciprocal space with the  $x$  and  $y$  axes in the directions parallel and perpendicular to the sample surface, respectively.

that the classical concepts of growth modes cannot explain our experimental results, instead we suggest that the V growth is governed by the so-called roughening transition of a crystal surface,<sup>18,20</sup> which is triggered by surface strain gradients associated with the presence of misfit dislocations.

#### A. The role of surface and interface energies

Using the arguments concerning the surface and interface energies outlined in the Introduction, the expected growth

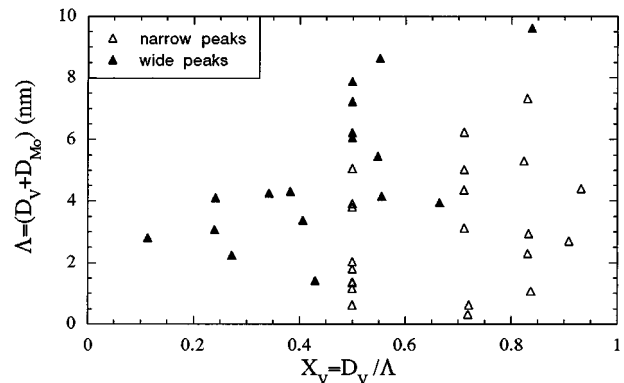


FIG. 8. Plot of the relative V-layer thickness  $X_V = D_V/\Lambda$  of each sample in this study vs  $\Lambda$ . The open and filled symbols show the  $\omega$  width of the XRD Bragg peak,  $\beta_\omega$ . Open triangles represent superlattices with  $\beta_\omega < 0.41^\circ$  and filled triangles represent superlattices with  $\beta_\omega > 0.41^\circ$ . The results in Fig. 3 lie on the line  $X_V = 0.5$ .

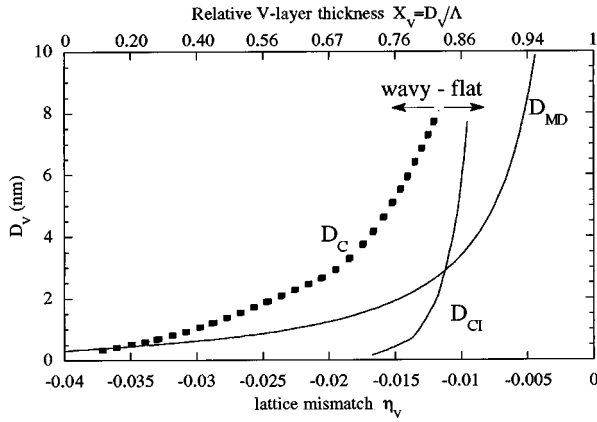


FIG. 9. The critical thicknesses for coherent 3D islanding ( $D_{CI}$ ) and misfit dislocation generation ( $D_{MD}$ ) plotted vs lattice mismatch  $\eta_V$ . The dotted line shows the experimentally determined critical thickness  $D_C$  as a function of the relative V-layer thickness  $X_V$ , labeled at the top of the diagram. The dotted line corresponds to the experimentally determined maximum thickness of 2D V layers as a function of the minimum possible lattice mismatch between V and the Mo/V superlattice substrate. The relationship between  $\eta_V$  and  $X_V$  was obtained through linear elasticity theory and under the assumption of no strain relaxation ( $\rho=0$ ).

modes of V on Mo and Mo on V were investigated. We found that V should nucleate and grow in a 2D mode up to a V-layer thickness of at least 30 nm on Mo. This is much larger than the thickness of a few monolayers that is usually found in SK systems and also larger than the critical thickness  $D_C$  experimentally observed in this work. Thus, for the V-layer thicknesses considered in this work ( $D_V < 10$  nm), interface and surface energies alone are not critical for changing the growth of V from wetting to nonwetting conditions. Moreover, a substantial bulk diffusion is required to turn such a thick film from a wetting to a nonwetting state. This is unlikely to occur at the used growth temperature  $T_s=973$  K, since interdiffusion has been observed experimentally to be negligible.<sup>28</sup> Based on these arguments we conclude that, at temperatures high enough to allow for an extensive surface diffusion but below the temperatures where bulk diffusion is activated, V will nucleate and grow as a 2D film up to a thickness of  $\sim 30$  nm. Our experimental results for V in Mo/V superlattices do not agree with this conclusion. V layers with a 3D surface morphology are observed at much smaller thicknesses, indicating that surface and interface energies play a minor role for the observed waviness in the studied superlattices.

Contrary to V on Mo, surface energy arguments indicate a strong driving force for a three-dimensional nucleation of Mo on V. However, we did not find any evidence of a pronounced island growth of Mo on V in our experiments. At short periods it is clear from the TEM images shown that the growth occurs in a 2D mode. Mo conformally covers the V surface even after the 2D-to-3D transition, indicating a 2D growth of Mo on each terrace of the V surface. Using the argumentation with surface and interface energies above, the wetting condition can never be fulfilled for a Mo film on a V substrate since  $\gamma_V - \gamma_{Mo} < 0$ . This indicates either that the surface energy is modified during growth of Mo or that the growth is governed by limited Mo surface diffusion, which

forces the Mo to nucleate as 2D islands or bind to the step edges. First, the high surface energy during growth of Mo can be lowered by the presence of impurities at the film surface, acting as a surfactant. For example, a reduction in the film surface energy can be achieved by surface segregation of a small amount of V to the surface of the growing Mo film. This kind of growth would require a high surface mobility of V and it would imply that Mo atoms penetrate the surface V layer and nucleate as the second atomic layer from the surface. As will be shown in Sec. IV C the growth temperature is above the so-called roughening temperature for V, which shows that the V surface diffusivity indeed is high. Secondly, initial cross-sectional TEM studies of single-crystal Mo/W(001) superlattices, grown under the same conditions as the Mo/V superlattices in the present work, showed a pronounced accumulated roughness,<sup>29</sup> implying that Mo growth is kinetically limited at  $T=970$  K. Thus, we conclude that the growth of Mo in the present Mo/V superlattices is governed by limited surface kinetics, possibly in combination with surface impurities that reduce the surface energy. The absence of accumulated roughness must then be due to the smoothening process during growth of V.

For the estimations in this section the surface energies  $\gamma_{Mo}$  and  $\gamma_V$ , at the growth temperature  $T_s$ , were calculated by the empirical rule given by Murr.<sup>30,31</sup> The interface energy  $\gamma_I$  was calculated as the sum of the energy increase  $E_i$ , due to an interface between regions of unlike atoms, and the energy  $E_D$ , associated with an interfacial square network of misfit dislocations.  $E_i$  was estimated by the equation  $E_i = \gamma_{Mo} + \gamma_V - 2\sqrt{\gamma_{Mo}\gamma_V}$ , which was obtained using the definition of the surface energy<sup>21</sup> and the Lorentz-Berthelot rule for the interatomic potential between unlike atoms.<sup>32</sup>  $E_D$  as a function of film thickness and lattice mismatch was calculated using the expression given by Matthews<sup>7</sup> assuming total strain relaxation of the film.

### B. 3D evolution due to coherency strain

Since surface and interface energy arguments alone are unable to explain the observed 2D-3D transition of V, we investigated if lattice relaxed Stranski-Krastanow or coherent 3D island growth can explain a 3D morphology evolution of V at the observed critical thicknesses. The transition thicknesses for both SK and CI growth depend on the lattice mismatch between the film and the substrate. The film is the last (growing) V layer while the substrate in this context is the topmost layer of Mo in the already deposited part of the superlattice. The lattice mismatch  $\eta_V$ , of V growing on a Mo/V superlattice, therefore depends on  $X_V$ , i.e., the relative amount of V in the superlattice, and the degree of coherency strain relaxation  $\rho_{Mo}$  of the topmost Mo layer. A large value of  $X_V$  and a small value of  $\rho_{Mo}$  (little relaxation) means that the lattice parameter of the substrate (the surface of the latest deposited Mo layer) in the plane of the surface is mostly guided by the V in the superlattice, which thus yields a small  $\eta_V$ . On the other hand, if  $X_V$  is small or if  $\rho_{Mo}$  is large, the V film will experience a large lattice mismatch. It should be noted that neither SK or CI growth can be expected to fully explain the 2D-3D transition of V since the layers were found to be at least partly relaxed at V thicknesses below  $D_C$  ( $\rho \approx 50\%$  in smooth, 2.5-nm-thick, V layers when

$X_V=0.5$ ). However, these phenomena cannot be excluded for other values of  $X_V$ . We have therefore estimated critical thicknesses for 3D surface evolution in SK and CI growth for  $\eta_V$  values ranging from 0 to  $\eta_0 = -3.9\%$ . Since the 2D-3D transition in SK growth is accompanied by MD generation, the critical thickness for MD generation  $D_{MD}$ , can be used as an approximation of the maximum transition thickness. We use the single-film model of Matthews<sup>7</sup> to calculate  $D_{MD}$  and  $D_{CI}$  was calculated using the dynamical model of Spencer, Voorhees, and Davis.<sup>14</sup>

The results of the calculations<sup>31</sup> are presented in Fig. 9 where  $D_{MD}$  and  $D_{CI}$  are shown together with the experimentally determined V-layer thickness  $D_c$  for the 2D to 3D growth transition.  $D_c$  is plotted versus the layer thickness ratio  $X_V$ , which is labeled at the top of the figure. The relation between  $X_V$  and  $\eta_V$  was obtained using linear elasticity theory assuming  $\rho_{Mo} = 0$ , which certainly is not true, at least not for the superlattice with  $D_V = D_c$  and  $X_V = 0.5$ , as is evident from the TEM results. The experimental curve thus represents the maximum thickness of a flat V film as a function of the minimum possible lattice mismatch between V and a Mo/V superlattice substrate with a given  $X_V$ . Note that  $\eta_V$  is negative since  $a_{0V}$  is smaller than  $a_{||Mo}$ .

As can be seen in Fig. 9,  $D_c$  coincides only with the critical thickness for MD generation when  $|\eta_V| \geq 0.035$ . Here  $D_c$  is about 0.5 nm ( $\sim 3$  monolayers), which is a typical thickness observed for the 2D-3D transition in SK systems. Thus, for small values of  $X_V$  (large  $|\eta_V|$ ), V may well grow in the classical SK mode. For smaller  $|\eta_V|$  values,  $D_{MD}$  is smaller than  $D_c$ , which is in line with our findings that the V layers are partly relaxed before the 2D-3D transition occurs. This also confirms that V does not grow in a classical SK mode in this type of superlattice. The  $D_{CI}$  curve is below both  $D_c$  and  $D_{MD}$  in the range of  $X_V$  investigated experimentally, suggesting that coherent 3D island growth should be the main relaxation mechanism. This is in contradiction with our experimental results and we thus conclude that the CI model used is not applicable to V on Mo at the given growth conditions. One possibility to qualitatively explain the observed 2D-3D transition at  $D_c$ , in the framework of coherent 3D islanding, is to allow for a certain degree of relaxation by MD's before the 3D surface evolution occurs. Such a "semicoherent" 3D islanding would be an intermediate growth mode between coherent 3D islanding and SK growth and would be in agreement with our observation that MD's are present at V-layer thicknesses below  $D_c$ . Although a theoretical description of "semicoherent" 3D islanding has, to our best knowledge, not been reported in the literature, it cannot be excluded as the mechanism for the waviness observed in this work.

Even if the preceding treatment certainly is oversimplified it demonstrates the sensitivity in surface and strain energy balances and qualitatively predicts the observed 2D nucleation behavior of V during growth of short period Mo/V superlattices. However, the subsequent 3D evolution of V cannot be explained by the classical models. This implies that the morphology of V is governed primarily by other driving forces than surface and coherency strain energies.

### C. 3D evolution due to the roughening transition

We conclude from the preceding section that the V layers in a Mo/V superlattice grow in a wetting mode and that the

layers relax by misfit dislocations without island evolution when  $|\eta_V| \leq 0.035$  and  $D_V < D_c$ . Stranski-Krastanow growth or coherent 3D islanding can not explain the waviness of the V layers as  $D_V$  exceeds  $D_c$ . Thus, another mechanism has to be employed in order to explain our results.

Roughening due to kinetically limited growth is unlikely since the diffusion length involved is estimated to be in the  $\mu\text{m}$  range (using Einstein's relation and the approximation of the surface diffusion coefficient described by Flynn<sup>33</sup>).

On the contrary, the high diffusivity indicates that the surface is above the so-called roughening temperature  $T_R$ .<sup>21</sup> At  $T_R$  no free energy is needed to form a surface vacancy or a kink at a step edge since the formation energy is exactly balanced by the entropy term. Below  $T_R$  the surface is basically flat with only small clusters of adatoms or surface vacancies present, whereas above  $T_R$  the surface diffusion is fast and arbitrarily large clusters can be found with a delocalized surface as a consequence.  $T_R$  is predicted to be higher for surfaces with closely packed atoms than for less dense surfaces since the formation energies of surface vacancies and kinks are larger for the more dense surfaces. The features of the roughening transition have been modeled by Monte Carlo simulations of surfaces described by so-called solid-on-solid models.<sup>20</sup> Even though determinations of  $T_R$  are rather rare, particularly for bcc metals,  $T_R$  was recently experimentally found to be 800 K for the  $\{110\}$  surfaces and 860 K for the  $\{100\}$  surfaces of single-crystal Ta.<sup>34</sup> These temperatures were determined by the observation of accelerated growth from the vapor phase on the faces of a field ion microscopy tip. The ratio between the melting temperature  $T_m$  and  $T_R$  is thus 0.24 for the  $\{110\}$  surfaces and 0.26 for the  $\{100\}$  surfaces of Ta. In the same paper the roughening temperature for  $\{110\}$  surfaces of W was quoted to be  $\sim 1000$  K, which corresponds to  $T_R/T_m \approx 0.27$ . Furthermore, in a recent Monte Carlo simulation of the B2 bcc  $\text{Fe}_{0.8}\text{Al}_{0.2}$  alloy the roughening temperature for the  $\{100\}$  surfaces of the alloy was found to be  $\sim \frac{1}{3}$  of the critical temperature which, in turn, is lower than  $T_m$ .<sup>35</sup> These values for bcc metals are surprisingly low compared to the experimentally determined  $T_R/T_m$  of 0.6–0.7 for the  $\{110\}$  surfaces of fcc metals<sup>36–38</sup> and the theoretical prediction for the  $\{100\}$  surfaces of simple cubic materials, which gives  $T_R/T_m = 0.54$ .<sup>20</sup> Analytical results also indicate that bcc metals have a  $T_R/T_m$  close to the value predicted for simple cubic crystals.<sup>39</sup> However, if we assume that the roughening temperatures for the Mo and V  $\{100\}$  surfaces are at least  $\sim 1/3 T_m$ , we obtain  $T_R^{Mo} \geq 960$  K and  $T_R^V \geq 720$  K, respectively.<sup>31</sup> These values should be compared to the growth temperature  $T_S = 973$  K for the superlattices. Thus, a wavy V surface can be expected since  $T_S > T_R^V$  while for Mo no conclusions can be drawn since  $T_S \approx T_R^{Mo}$ . Furthermore, the observed absence of accumulated roughness in the superlattices can also be understood in terms of the roughening transition. If there is no lateral variation in the chemical potential  $\mu$ , due to, e.g., surface roughness of the previous layer or MD's at the V/Mo interface, then there will be no correlation between the surfaces of two neighboring V layers.

We conclude that the roughening transition can explain the observed 3D evolution of the V surfaces as well as the

absence of accumulated roughness in the superlattices. However, it does not explain the smoothening effect, nor the strain-dependent critical thickness.

#### D. Surface migration due to lateral variations in the chemical potential

Since both roughening and smoothening involve a significant surface migration of atoms, we have estimated how MD-induced surface strain and curvature influences the lateral variations of the chemical potential  $\mu$ . We used the elastic continuum model presented by Freund, Beltz, and Jonsdottir,<sup>15</sup> where the lateral variation of chemical potential  $\mu = \mu(x)$  as a function of curvature and surface strain  $\varepsilon$  is given by

$$\mu(x) = [U(\varepsilon(x)) - \kappa(x)\gamma] \times \Omega, \quad (1)$$

where  $U(\varepsilon) \propto \varepsilon^2$  is the strain energy density,  $\kappa$  is the curvature of the surface (which is positive if the surface is concave to the normal direction),  $\gamma$  is the surface energy, and  $\Omega$  is the atomic volume. Thus, in the absence of lateral strain variations, Eq. (1) describes the smoothening due to curvature;<sup>40,41</sup> i.e., the chemical potential on a wavy surface varies such that mobile surface atoms are driven from regions with negative curvature (“ridges”) down to regions with positive curvature (“depressions”). On the other hand, if the surface is flat and the surface strain varies along the surface, there will be a driving force for roughening. Thus a periodically varying strain field due to a MD network in a 2D layer may alone lead to a transition from a 2D to a 3D surface.

Taking a 2D V layer with  $D_V = 2.5$  nm on a Mo/V superlattice with  $X_V = 0.5$  and  $\rho = 50\%$  as an example of our calculations<sup>31</sup> (corresponding to the situation in Fig. 4), we found that the curvature term,  $\kappa(x)\gamma$  Eq. (1), is large in magnitude and negative,  $\sim -10^{10}$  Pa,<sup>15</sup> while the strain term is positive and on the order of  $10^7$  Pa right above each dislocation. Midway between the two dislocations  $U(\varepsilon)$  is on the order of  $10^8$  Pa while  $\kappa(x)\gamma$  now is positive but smaller in magnitude than  $U(\varepsilon)$ . This yields chemical potentials of  $\mu \approx 1$  eV per atom right above the MD’s and  $\mu \leq 10$  meV per atom in-between the dislocations *before* any roughening has taken place. Thus, due to the presence of MD’s there is a gradient of the chemical potential along the surface that provides a strong driving force for creating surface vacancies and steps. This gradient can be expected to increase with decreasing distance between the dislocations.

On the other hand, if V is grown coherently on an already wavy Mo surface, the surface diffusion will be governed only by the curvature. This means that, initially, V will have a higher growth rate in the depression and can, before MD’s are formed, eventually planarize the surface.

We conclude this section by noting that  $\mu$  does vary in a way such that there is a driving force for smoothening if growth occurs on a wavy surface while roughening can be expected when the MD density becomes large enough in flat layers.

#### V. SUMMARY AND CONCLUDING REMARKS

Based on the above discussion we can now propose possible explanations for (i) the transition from smooth V layers

to layers with large in-plane thickness fluctuations as  $D_V$  exceeds  $D_c$ , (ii) the  $X_V$  dependence of  $D_c$ , (iii) the smoothening process responsible for the nonaccumulative surface roughness, and (iv) the conformal coverage of Mo on the wavy V surface.

(i) In the initial stage of growth, i.e., for V-layer thicknesses  $< 30$  nm, a V film wets a Mo surface due to the large difference in surface energies between Mo and V. Although V is predicted to grow above its roughening temperature, no roughening seems to occur until the V layers have achieved a certain thickness  $D_c$ . The reason can be that our estimated  $T_R^V$  for the  $\langle 100 \rangle$  surfaces may be too low. If this is the case, the increasing number of MD’s, created upon relaxation as the film grows, will cause a gradient of the chemical potential along the flat surface that provides a strong driving force for creating surface vacancies and steps above each MD. Surface material will be transported away from the regions above the dislocations to areas in between the dislocations. We propose that this is the mechanism that triggers the 2D-3D transition. Once the surface starts to be corrugated by the presence of MD’s, faces with less densely packed surfaces are created. These faces have a lower energy for creation of steps, which means that they have a lower roughening temperature than the (001) surface with an acceleration of the roughening rate as a consequence.

(ii) The reason the onset of 3D evolution occurs at thicknesses far beyond  $D_{MD}$  can again be understood if the growth temperature is lower than  $T_R^V$  for the (001) surface, but higher than the roughening temperatures for other less densely packed (high-index) surfaces. If this is the case, the roughening will not take place unless a high-index face (with lower  $T_R$ ) is created on the surface, but once this has occurred the surface roughening evolves precipitously. The increase in  $D_c$  with increasing  $X_V$  is a combined effect of the increased critical thickness for MD generation and the reduced surface strain and curvature due to these dislocations when they are located far from the surface.

(iii) The fact that smooth layers can be obtained again during growth by reducing  $D_V$  to a value below  $D_c$  shows that V preferably nucleates in the depressions of a wavy Mo surface. An increased local growth rate can indeed be expected in these regions due to the large number of step edges that provide favorable nucleation sites at the slopes. Furthermore, before any MD’s are formed, the gradient in the chemical potential will be governed by the curvature, which then leads to a mass transport from ridges down into depressions and thus to a smoothening effect. When the depressions are filled, the V layer will be smooth and continuous, but with a nonuniform thickness. From this stage, smooth layers can continue to grow provided that  $X_V$  is kept at a value such that  $D_V$  is below  $D_c$ . If not so, MD formation can again trigger the 3D surface evolution.

(iv) The observed conformal Mo coverage of the uneven V layers is either due to a low surface mobility of Mo or due to an impurity related lowering of the surface energy that leads to a 2D growth mode. This experimental observation also implies that  $T_R^{Mo}$  is higher than the growth temperature used,  $T_m = 973$  K. The observation that the roughening does not accumulate with increasing superlattice thickness is a

consequence of the delocalized surface of the growing V film above  $T_R^V$ , i.e., there is no memory effect about the roughness between successive V layers. This 3D morphology is frozen-in in the superlattices by capping the undulated V layers with Mo, which leads to a “lasagne-like” structure as seen in Fig. 5.

#### ACKNOWLEDGMENTS

The financial support from the Swedish NUTEK/NFR materials research consortium for Thin Film Growth and the Swedish National Research Council (NFR) is highly appreciated. G.R. acknowledges the support of an OTKA 1222 grant of the Hungarian National Science Foundation.

\*Present address: ESRF, B.P. 220, F-38 043 Grenoble, France; electronic address: birch@esrf.fr

- <sup>1</sup>R. Bruinsma and A. Zangwill, *Europhys. Lett.* **4**, 729 (1987).
- <sup>2</sup>M. H. Grabow and G. H. Gilmer, *Surf. Sci.* **194**, 333 (1988).
- <sup>3</sup>J. A. Venables, G. D. T. Spiller, and M. Hanbücken, *Rep. Prog. Phys.* **47**, 399 (1984).
- <sup>4</sup>R. Hull and J. C. Bean, *Crit. Rev. Solid State Mat. Sci.* **17**, 507 (1992).
- <sup>5</sup>D. J. Eaglesham and M. Cerullo, *Phys. Rev. Lett.* **64**, 1943 (1990).
- <sup>6</sup>M. Gendry, V. Drout, C. Santinelli, and G. Hollinger, *J. Vac. Sci. Technol. B* **10**, 1829 (1992).
- <sup>7</sup>J. W. Matthews, *J. Vac. Sci. Technol.* **12**, 126 (1975).
- <sup>8</sup>F. K. LeGoues, M. Copel, and R. Tromp, *Phys. Rev. Lett.* **63**, 1826 (1989).
- <sup>9</sup>B. W. Dodson, *Surf. Sci.* **184**, 1 (1987).
- <sup>10</sup>C. W. Snyder, J. F. Mansfield, and B. G. Orr, *Phys. Rev. B* **46**, 9551 (1992).
- <sup>11</sup>C. W. Snyder, B. G. Orr, D. Kessler, and L. M. Sander, *Phys. Rev. Lett.* **66**, 3032 (1991).
- <sup>12</sup>G. Springholz and G. Bauer, *Phys. Rev. B* **48**, 10 998 (1993).
- <sup>13</sup>D. J. Srolovitz, *Acta Metall.* **37**, 621 (1989).
- <sup>14</sup>B. J. Spencer, P. W. Voorhees, and S. H. Davis, *Phys. Rev. Lett.* **67**, 3696 (1991).
- <sup>15</sup>L. B. Freund, G. E. Beltz, and F. Jonsdottir, in *Thin Films: Stresses and Mechanical Properties IV*, edited by P. H. Townsend *et al.*, MRS Symposia Proceedings No. 308 (Materials Research Society, Pittsburgh, 1993), p. 383.
- <sup>16</sup>A. P. Payne, W. D. Nix, B. M. Lairson, and B. M. Clemens, *Phys. Rev. B* **47**, 13 730 (1993).
- <sup>17</sup>B. G. Orr, D. Kessler, C. W. Snyder, and L. Sander, *Europhys. Lett.* **19**, 33 (1992).
- <sup>18</sup>W. K. Burton, N. Cabrera, and F. C. Frank, *Philos. Trans. R. Soc. London Ser. A* **234**, 299 (1951).
- <sup>19</sup>P. Bennema, *J. Phys. D* **26**, B1 (1993).
- <sup>20</sup>J. D. Weeks and G. H. Gilmer, in *Advances in Chemical Physics*, edited by I. Prigogine and S. A. Rice (Wiley, New York, 1979), p. 157.
- <sup>21</sup>A. Zangwill, *Physics at Surfaces* (Cambridge University Press, Cambridge, 1988).
- <sup>22</sup>G. Håkansson, J. Birch, L. Hultman, I. P. Ivanov, J.-E. Sundgren, and L. R. Wallenberg, *J. Cryst. Growth* **121**, 399 (1992).
- <sup>23</sup>J. Birch, M. Severin, U. Wahlström, Y. Yamamoto, G. Radnoczi, R. Riklund, J.-E. Sundgren, and L. R. Wallenberg, *Phys. Rev. B* **41**, 10 (1990).
- <sup>24</sup>J. Birch, J.-E. Sundgren, and P. F. Fewster, *J. Appl. Phys.* **78**, 6562 (1995).
- <sup>25</sup>D. J. Miller, K. E. Gray, R. T. Kampwirth, and J. M. Murduck, *Europhys. Lett.* **19**, 27 (1992).
- <sup>26</sup>K. Järrendahl, J. Birch, L. Hultman, L. R. Wallenberg, G. Radnoczi, H. Arwin, and J.-E. Sundgren, in *Amorphous Silicon Technology—1992*, edited by M. J. Thompson *et al.*, MRS Symposia Proceedings No. 258 (Materials Research Society, Pittsburgh, 1992), p. 571.
- <sup>27</sup>E. E. Fullerton, I. K. Schuller, and Y. Bruynseraede, *MRS Bull.* **XVII**, 33 (1992).
- <sup>28</sup>J. Birch, Y. Yamamoto, G. Radnoczi, J.-E. Sundgren, and L. R. Wallenberg, *Vacuum* **41**, 1231 (1990).
- <sup>29</sup>E. B. Svedberg, M.Sc. thesis, Linköping University, Sweden, 1993.
- <sup>30</sup>L. E. Murr, *Interfacial Phenomena in Metals and Alloys* (Addison Wesley, Reading, MA, 1975).
- <sup>31</sup>The following values of the material properties were used for the calculations in this paper: melting temperatures;  $T_{m,Mo}$  = 2888 K, and  $T_{m,V}$  = 2173 K, surface energies at  $T_m$ ;  $\gamma_{m,Mo}$  = 2250 mJ/m<sup>2</sup>, and  $\gamma_{m,V}$  = 1950 mJ/m<sup>2</sup>, lattice parameters  $a_{Mo}$  = 0.31469 nm, and  $a_V$  = 0.30232 nm; shear modulus  $G_V$  = 54 GPa, Poisson ratio  $\nu_V$  = 0.26, and burgers vector  $b$  = 2.13.
- <sup>32</sup>M. P. Allen and D. J. Tildesley, *Computer Simulation of Liquids* (Clarendon, Oxford, 1987).
- <sup>33</sup>C. P. Flynn, *J. Phys. F* **18**, L195 (1988).
- <sup>34</sup>R. Vanselow and X. G. D. Li, *Surf. Sci. Lett.* **281**, L326 (1993).
- <sup>35</sup>F. Schmid and K. Binder, *Phys. Rev. B* **46**, 13 (1992).
- <sup>36</sup>G. Bracco, C. Malo, C. J. Moses, and R. Tatarek, *Surf. Sci.* **287-288**, 871 (1993).
- <sup>37</sup>U. Romahn, P. von Planckenhagen, C. Kroll, and W. Gopel, *Phys. Rev. B* **47**, 12 (1993).
- <sup>38</sup>H. Hornis, J. D. West, E. H. Conrad, and R. Ellialtioglu, *Phys. Rev. B* **48**, 14 (1993).
- <sup>39</sup>H. van Beijeren, *Phys. Rev. Lett.* **38**, 993 (1977).
- <sup>40</sup>W. W. Mullins, in *Metal Surfaces: Structure, Energetics and Kinetics*, edited by W. D. Robertson and N. A. Gjostein (American Society for Metals, Metals Park, 1963), p. 17.
- <sup>41</sup>P. Shewmon, *Diffusion in Solids* (TMS, Warrendale, 1989).